Acta Materialia 232 (2022) 117932

Contents lists available at ScienceDirect

Acta Materialia

journal homepage: www.elsevier.com/locate/actamat

Full length article

White etching bands formation mechanisms due to rolling contact fatigue

Mostafa El Laithy[a,*], Ling Wang[a], Terry J. Harvey[a], Alexander Schwedt[b], Bernd Vierneusel[c], Joachim Mayer[b]

[a] National Center of Advanced Tribology at Southampton (nCATS), University of Southampton, University Road, Southampton SO17 1BJ, UK
[b] Central Facility for Electron Microscopy (GFE), RWTH Aachen University, Ahornstraße 55, 52074 Aachen, Germany
[c] Schaeffler Technologies AG & Co. KG, Georg-Schäfer-Straße 30, 97421 Schweinfurt, Germany

ARTICLE INFO

Article history:
Received 29 October 2021
Revised 1 February 2022
Accepted 6 April 2022
Available online 19 April 2022

ABSTRACT

Subsurface micro-structural changes such as dark etching region (DER) and white etching bands (WEB) which develop in bearing steels due to cyclic stresses in rolling contacts, have been studied for decades and a number of theoretical models have been proposed to explain their formation mechanisms and predict their initiation. In WEB investigations, studies have generally focused only on one subtype of WEB, e.g. low angle bands (LAB) or high angle bands (HAB), while the most recent semi-empirical model has shown to be able to predict the formation of both LAB and HAB based on observed growth patterns of ferrite grains. Following from the modelling study, this paper presents a detailed mechanistic study, showing the evolution of ferrite grains (equiaxed and elongated grains) and carbide structures in WEB formed in inner rings of angular contact ball bearings at their different life stages through SEM, EBSD and nano-indentation analysis. The results strongly suggest both LAB and HAB initiate as equiaxed ferrite grains due to recrystallization arising from energy build-up in the initial microstructure that later develops to elongated ferrite grains through a grain rotation/coalescence recovery mechanism induced from plastic deformation. The formation of carbide structures in LAB is associated with the transformation of equiaxed to elongated grains, where carbides nucleate at the edges of the elongated grains rather than at the equiaxed grain band edges as being previously suggested in literature. The newly proposed formation mechanism links LAB and HAB based on experimental findings from detailed inspection of gradual microstructural alteration sequence of LAB and HAB in rolling contact fatigue (RCF) tested bearings.

© 2022 The Author(s). Published by Elsevier Ltd on behalf of Acta Materialia Inc.
This is an open access article under the CC BY license (http://creativecommons.org/licenses/by/4.0/)

1. Introduction

Increasing the resistance of bearing steels to rolling contact fatigue (RCF) plays an important role in rolling bearing industry. RCF is caused by cyclic contact stresses in the bearing rolling elements and raceways during operation and is usually manifested by subsurface microstructural alterations commonly known as dark etching regions (DER) and white etching bands (WEB). Detailed knowledge of the formation mechanism and properties of these features and their role in crack formation will support the development of future bearing steels and better RCF prediction models.

Development of the RCF-induced microstructural alterations typically begins with the formation of DER, which appears as randomly distributed dark patches in the parent martensite matrix within the maximum shear stress regions after being etched in optical images [1–4]. DER is typically found to form from over 5 million stress cycles depending on the contact pressure [5,6,2,7]. It has been proposed that DER forms due to carbon migration from parent martensite to heavily dislocated regions and nano-sized tempered carbides leading to the formation of ferrite grains [1,2,8,9]. A recent study has shown that DER consists of equiaxed and elongated ferrite structures with the former being developed through recrystallization [10]. However, the evolution of these structures during the bearing life remains unclear.

WEB develop later in the bearing life compared with DER and within the maximum shear stress region [3]; and have typically been found to be within the DER. However, DER is not seen as the pre-requisite of WEB, e.g. they have been found to form without DER when steels are tempered to a hardness below 720 HV [11,12]. The density of WEB formed in bearings is found to increase with the stress cycle and HAB formation follows LAB [3,13]. Based on fully formed WEB, a previous study has shown that the ferrite

* Corresponding author.
E-mail address: mel2g13@soton.ac.uk (M. El Laithy).

https://doi.org/10.1016/j.actamat.2022.117932
1359-6454/© 2022 The Author(s). Published by Elsevier Ltd on behalf of Acta Materialia Inc. This is an open access article under the CC BY license (http://creativecommons.org/licenses/by/4.0/)

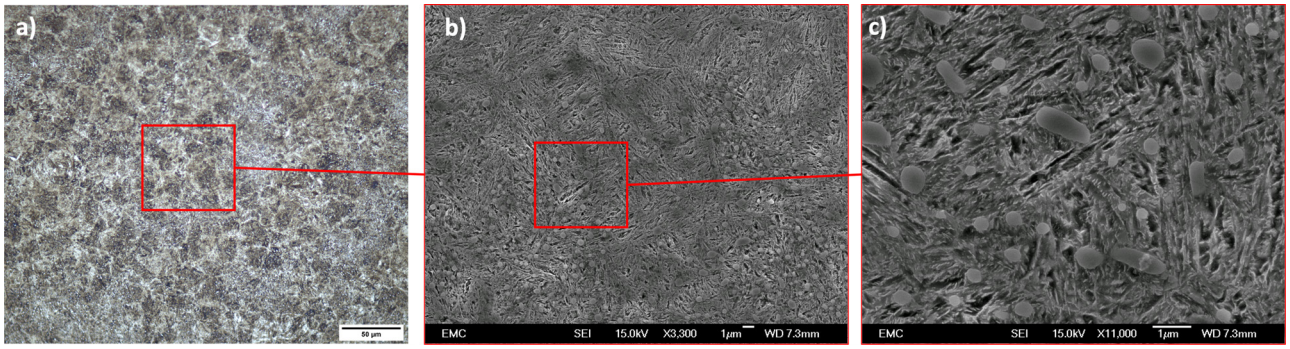

Fig. 1. Images showing the microstructure of the 100C6 steel from a virgin ACBB a) an optical microscope image, b) an SEM image of the area highlighted in a), c) an SEM image at higher magnification of the area highlighted in b).

grains (both equiaxed and elongated grains) have a general alignment of a <111> axis parallel to the over-rolling normal direction (normal to rolling direction) and based on the Gamma-fibre textures and higher EBSD pattern quality in the ferrite grains comparing with that of the parent martensite microstructure, it was suggested that recrystallization contributes to the formation of the WEB [10]. However, no detailed discussions on what conditions lead to their formation was given. The same study has also suggested that the elongated ferrite grains are deformation induced based on the evidence that a <111>{112} slip system is found to be aligned with the elongated ferrite grain long axis direction in both LAB (~30° to rolling direction) and HAB (~80° to rolling direction).

One of the earliest studies on LAB by Buchwald et al. suggested that carbon migration occurs due to a stress gradient in localized plastic deformation regions leading to dilational compressive strains, which dissolves the existing precipitates [14]. This results in the development of LAB ferrite bands in this region supersaturated with carbon. They suggested that the resulting carbon concentration gradient within the band due to the dissolved precipitates acts as a driving force for the migration of carbon from the ferrite band to the edge of the band where carbide nucleation occurs. Polonsky et al. then proposed that the driving force for carbon migration was the stress induced by the release of carbon segregated at dislocations within equiaxed ferrite [15]. They suggested that dislocation annihilation in the equiaxed ferrite has led to accumulation of free carbon solute in the band (equiaxed ferrite). As the free carbon concentration in the band increases due to continuous dislocation annihilation, a concentration gradient is created driving the diffusion of carbon to the edge of the band and the nucleation of carbide at the edge of the band. The most recent theory by Fu et al. proposed that carbon exists in Cottrell atmospheres within the equiaxed ferrite band, and during continuous cyclic loading, dislocation gliding within a ferrite band results in carbon migration from the ferrite band to its edge and carbide nucleation and growth [9]. Despite the various drivers proposed for the carbon migration during LAB formation in literature, it is generally in agreement that carbon migration across fully developed ferritic LAB to the ferrite-martensite interface results in lenticular carbides nucleation and growth. All proposed formation mechanisms in literature to date are based on LAB consisting of two microstructural constituents: equiaxed ferrite grains and lenticular carbides. The new findings of elongated ferrite grains in WEB [10] demands an updated theory to explain their formation mechanisms.

HAB have not been widely investigated so far especially in their relation to their formation mechanisms, mainly due to their formation at a much later stage in bearing life and require much more resources to investigate, e.g. thousands of hours of RCF tests.. It is generally accepted that HAB formation require pre-existing LAB development based on their formation sequence [6]. However little evidence has been seen in literature apart from those from the recent studies conducted by the authors group [3,13], where a link between the formation of HAB and the density of LAB has been shown.

This paper focuses on the analysis of microstructures of LAB and HAB at different formation stages using SEM, EBSD to elucidate the formation and evolution mechanisms of WEB as well as links between LAB and HAB. Nanoindentation tests are conducted to examine the hardness of each individual features within LAB and HAB, providing further evidence for their formation mechanism investigation.

2. Methodology

The investigation of WEB in this study has been conducted on angular contact ball bearings (ACBBs) of type 7205-B subjected to RCF testing on an L-17 bearing test rig at Schaeffler Technologies [16]. Bearing samples cut from RCF tested ACBB inner rings are examined using microscopy techniques following standard metallography procedure [3]. The 100Cr6 bearing steel used in the ACBB rings was martensitic hardened to 830 HV with S0-stabilization (industrial standard heat treatment set by controlling annealing temperatures to achieve dimensional stability at operating temperatures $\leq$ 150 °C). The composition of the steel is shown in Table 1 is obtained using spark emission spectroscopy. The microstructure of the steel samples is a typical martensitic structure consisting of $<$ 5% retained austenite.

2.1. RCF testing

RCF testing was performed under two different contact pressures of 2.9 GPa and 3.5 GPa over a range of pre-determined stress cycles to investigate WEB (LAB and HAB) from early to fully developed stages. Results from representative bearings (listed in Table 2) are presented in this paper to avoid being overwhelmed by the significantly large amount of information obtained from this study. Details of the test rig information can be found in [17]. A virgin bearing i.e. not being RCF tested, has also been studied for comparison. All bearings were tested at a viscosity ratio κ of 2.69 (ratio of operating viscosity to reference viscosity). No surface damage is observed in the bearings presented here after the RCF test.

2.2. Microstructural characterization procedure

A standard metallography procedure was employed for sample preparation and microstructure characterisation, including the successive mechanical polishing of bearing cut samples using 6 μm,

Table 1
Chemical Composition of the 100Cr6 bearing steel.

	Weight % (Wt%)								
Material	C	Si	Mn	P	S	Cr	Ni	Mo	Al
100Cr6	0.93	0.3	0.34	0.01	0.004	1.49	0.02	0.005	0.003

Table 2
A summary of the ACBBs investigated in this study

Material	Contact Pressure (GPa)	Stress Cycles for Inner Ring (Million)
100Cr6	-	0*
	3.5	151
		679
	2.9	591
		1116
		1689
		3016
		4141

* This is a virgin bearing.

3 µm, 1 µm and 0.25 µm diamond suspensions. The polished surfaces were then etched with 2% Nital to highlight the microstructural alterations in the samples. Etched samples were then examined under a JEOL JSM-6500F SEM with an accelerating voltage of 15 kV, followed by an EBSD examination on selected samples after re-polishing using a JEOL JSM-7000F SEM (equipped a EDAX Pegasus EBSD system) for grain structure analysis. Nano-indentation has been performed on selected samples using a NanoTest Vantage (Micro Materials Ltd.) nano-indentation system with a Berkovich tip to obtain the nano hardness of the features of interests related to WEB. Prior to nano-indentation and EBSD analysis, the etched surfaces were re-polished using colloidal silica suspension (OP-S) to obtain a deformation-free surface with minimal surface roughness in accordance with BS EN ISO 14577-1:2015 standards. The maximum penetration depth for nanoindentation has been controlled at 50 nm with a fixed load/unloading rate of 0.075 mN/s. A 45 s dwell time at maximum load was used and thermal drift correction data was enabled with a collection time of 45 s. The EBSD analysis includes the investigation of the microstructure using Inverse Pole Figure (IPF) map to determine grain orientations, Kernel Average Misorientation (KAM) map to determine misorientation of individual grains, Image Quality (IQ) map to indicate density of defects in different grains and High-Angle Grain Boundary (HAGB) map to detect new grain formation.

3. Results

Fig. 1 shows an optical and two SE SEM images of a sample from a virgin 100Cr6 ACBB, showing a typical plate and lath martensite microstructure containing spherical primary carbides.

3.1. LAB evolution

This section presents the microstructural features in LAB observed in a range of bearing samples, demonstrating its formation and evolution mechanisms. Based on the development of three microstructural alteration features, i.e. equiaxed grains, elongated grains and lenticular carbides [10], it is found to develop in three stages.

3.1.1. Early stage LAB

During the initial and early stage, LAB is found to contain short (<10 µm in length) single equiaxed bands as shown in Fig. 2, especially in bearings a) after low stress cycles (<1000 million cycles) (Fig. 2 a-c) and b) at the LAB boundaries in samples after high stress cycles (>1000 million cycles) (Fig. 2 d-i). At this stage, the bands are of a few µm in length and less than 1 µm in width, and consist of only equiaxed ferrite grains (indicated by the red arrows in Fig. 2). Confirmation of the grain structure is given in the EBSD results presented in Section 3.2. This agrees with previous findings that LAB formation is heavily influenced by the contact pressure at the bearing contacts or subsurface shear stresses and that the density of LAB follows the distribution of the shear stresses in the subsurface, suggesting that LAB formed at the boundaries of the WEB region are at an earlier stage than those in the middle of the region [3,13]. The growth of equiaxed ferrite bands in length and thickness is found to involve dissolution of an adjacent primary carbide (see green circle highlighting a dissolving spherical carbide in Fig. 2e).

3.1.2. Intermediate stage LAB

Following from the early stage single equiaxed bands, as the band grows, elongated grains are seen to initiate within the bands accompanied by the initiation and growth of lenticular carbides adjacent to the elongated grains (see images in Fig. 3), marking the beginning of the intermediate stage of LAB. The elongated ferrite grains are thin needle-like structures appearing as groove or crack-like structures under SEM due to etching [10] (yellow arrows in Fig. 3b and 3d) while the lenticular carbides are the smooth bright structures adjacent to the elongated grains due to their resistance to etching, indicated by red arrows in Figs. 3b and 3d. The lenticular carbides are also seen to grow in both length and thickness on both sides of the elongated grain.

As the stress cycle increases, both elongated ferrite grains and the adjacent lenticular carbides continue to grow across the equiaxed ferrite band until a 'cotton-bud' shape is formed, where equiaxed ferrite grains form the 'heads' and the elongated ferrite grain and lenticular carbides form the stem (see Fig. 3e and Fig. 3f). The lenticular carbides areas appear to be very smooth possibly due to its carbon-rich nature [10].

3.1.3. Late Stage LAB

At the late stage, single bands start to 'multiply' and LAB become 'clusters' of much thicker and longer bands (see examples given in Fig. 4). By this stage, it is difficult to identify any single bands, as they have grown into each other forming large LAB areas. However, the three features observed in the first two stages, i.e. equiaxed ferrite grains, elongated ferrite grains and lenticular carbides, are still in the LAB clusters (indicated by different colours of arrows in Fig. 4). . Same as that in earlier stages, lenticular carbides are found to be adjacent to elongated ferrite grains. This confirms that lenticular carbides do not form in equiaxed ferrite grains structures but form accompanying the formation of elongated ferrite grains. As shown in Fig. 4, elongated ferrite grains are thin dark needles within the region of equiaxed grains and their thickness varies from 30 to 400 nm (see in Fig. 4b) which is much thinner than the width of the equiaxed ferrite grain bands (range 2 to 8 µm) that make up most of the LAB.

3.2. EBSD analysis of LAB

Fig. 5 presents SEM/EBSD images of LAB from a bearing sample tested under 2.9 GPa for 3016 million cycles, showing both an early-stage LAB (solid circle) and a relatively late stage (dashed circle) LAB. Combining information from the BSE/SE SEM with the

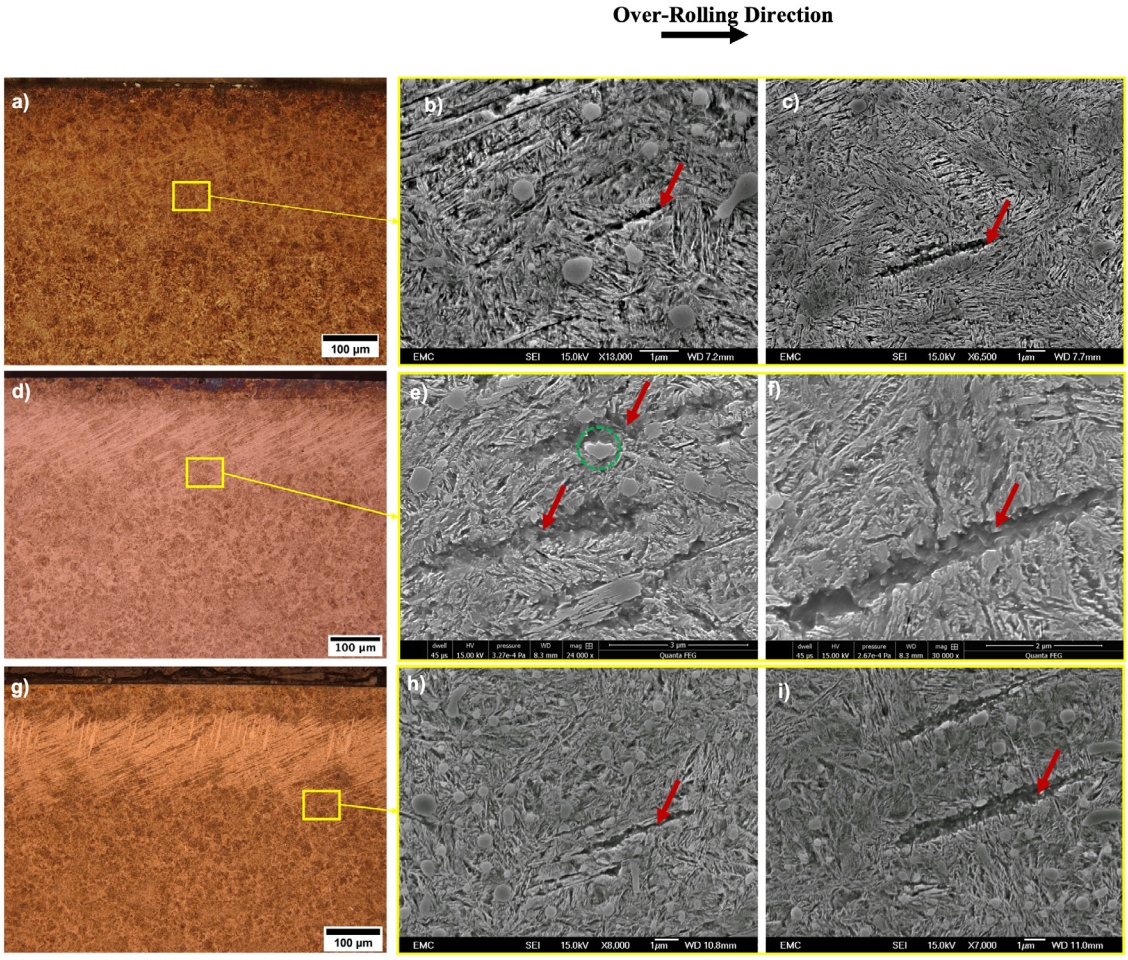

Fig. 2. Images of early stage LAB a) in a sample under 3.5 GPa for 679 million cycles. b) & c) SEM images from the region highlighted in a). d) In a sample under 2.9 GPa for 1116 million cycles. e) & f) SEM images from the region highlighted in d) with LAB from the lower boundary of the WEB region. g) In a sample under 2.9 GPa for 3016 million cycles. h) & i) SEM images from the region highlighted in g) with LAB from the lower boundary of the WEB region. Green area shows the dissolution of a primary carbide. Boundaries of the single bands are highlighted by yellow dotted line in b),c),e),f),h) and i).

IPF, KAM, IQ and HAGB maps, all captured for the same area, it can be seen that equiaxed grains appear to have various orientations (Fig. 5b) and a relatively high IQ contrast compared to the surrounding matrix (Fig. 5d) and low misorientation (Fig. 5c). This suggests there are less defects in these grains. The elongated grains, however, are shown to be much coarser comparing with the equiaxed grains with the long axis parallel to the band orientation of ~30° for LAB. It has also been found that elongated grains developed a texture close to <111> axis parallel to the normal direction (ND) (see in Fig. 5b). The elongated grains also show to have higher misorientation than that of the equiaxed grains (Fig. 5c) as it transferred from the blue equiaxed grains to green elongated grains, suggesting that the elongated grains are under the influence of a shearing component that contributes to the deformation of the grains. It should be noted that lenticular carbides have not been indexed under EBSD analysis (appear black in EBSD maps) which is likely due to the carbide crystallite size being smaller than the resolution of the EBSD.

3.3. HAB evolution

During later stages of LAB, HAB initiate and grow in the dense region of LAB [3], which coincides with the maximum shear stress region in the bearing subsurface [13]. The HAB as shown in Fig. 6, also consists of equiaxed and elongated grains similar to those in LAB with relatively larger dimensions, while during the earliest stage, HAB (see in Fig. 6a) only consists of equiaxed grains. At a later stage, small elongated grains appear to form within the equiaxed grain band of larger HAB (pointed by red arrows in Fig. 6b,c). As HAB grows, the elongated grains grow to be more pronounced (e.g. grows in length) (Fig. 6d,e). In the meantime, the number of elongated grains also increases and grows in parallel (seen in Fig. 6c-e within a single HAB). This is similar to the late stage development of LAB discussed previously. While the HAB shows a similar formation process involving equiaxed and elongated grain development as that in LAB, there is no lenticular carbides forming adjacent to the elongated grains (Fig. 6). Instead, carbides are found to cumulate at the edges of HAB, which can be easily observed in Figs. 6b-e.

During the early stage of HAB formation, equiaxed grains form in dense LAB regions while most of the lenticular carbides and elongated grains of the LAB are still visible (Fig. 6a). They are seen to gradually dissolve within the growing HAB i.e. individual HAB grows in both thickness and length during its intermediate stage (Fig. 6b). The LAB features remain intact outside the HAB. As the HAB continue to grow, lenticular carbides in the LAB cumulate and merge at the boundaries of HAB (see in Fig. 6c-e), marking the late stage of HAB formation. This suggests that the lenticular carbides of LAB located at the edge of the HAB act as carbon sinks for carbon in the HAB equiaxed and elongated grains to migrate to, forming a smooth and clear boundary between the equiaxed

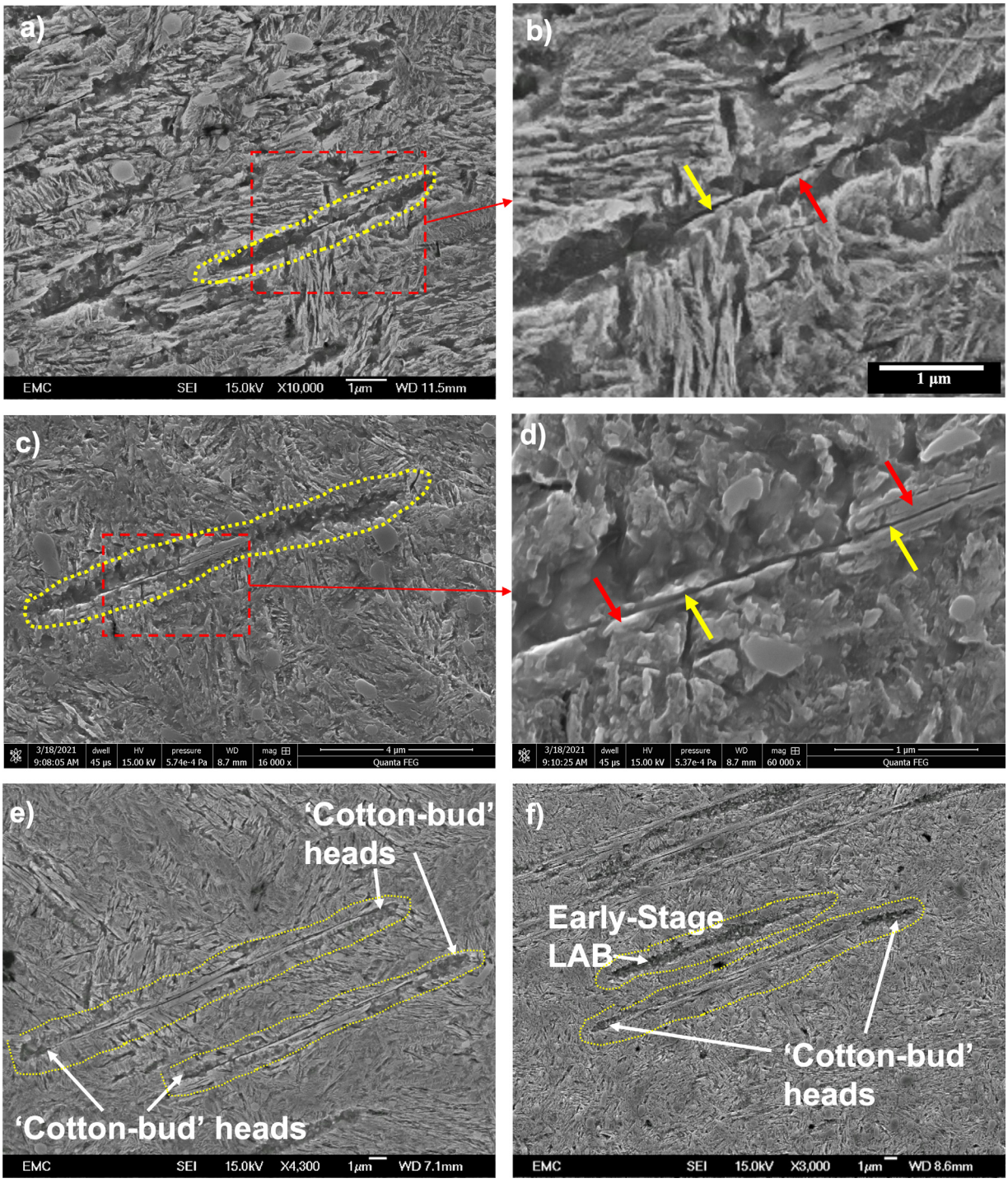

Fig. 3. Images of intermediate stage LAB from samples under 2.9 GPa for, a&b) 591 million cycles, c&d) 1116 million cycles, showing elongated ferrite grains formed in the middle of an LAB of equiaxed grains and lenticular carbides initiated adjacent to the elongated grains (in c) as well much developed lenticular carbides (in d). Yellow arrows point towards the elongated grains and red arrows indicate lenticular carbides structures. Cotton bud shape of LAB is shown from samples under 2.9 GPa for e) 3016 million cycles and f) 4141 million cycles where the heads consist of equiaxed grains and the stem consist of elongated grains and lenticular carbides. Boundaries of LAB in SEM images is highlighted in dotted line.

region of HAB and the newly formed lenticular carbides eventually (indicated in Fig. 6e). Thus there is no new lenticular carbides forming adjacent to the elongated grains within in the HAB in the similar way in LAB. As multiple HAB form, it reaches its final stage (see in Fig. 6f). The distance between individual HAB at this stage varies from 2 to 10 μm as shown in Fig. 6f.

3.4. EBSD analysis of HAB

Fig. 7a shows a BSE SEM image of HAB from a bearing sample tested under 2.9 GPa for 3016 million cycles while Fig. 7b-e presents the different EBSD analysis of the area highlighted in Fig. 7a at a higher resolution. To compare with the images shown

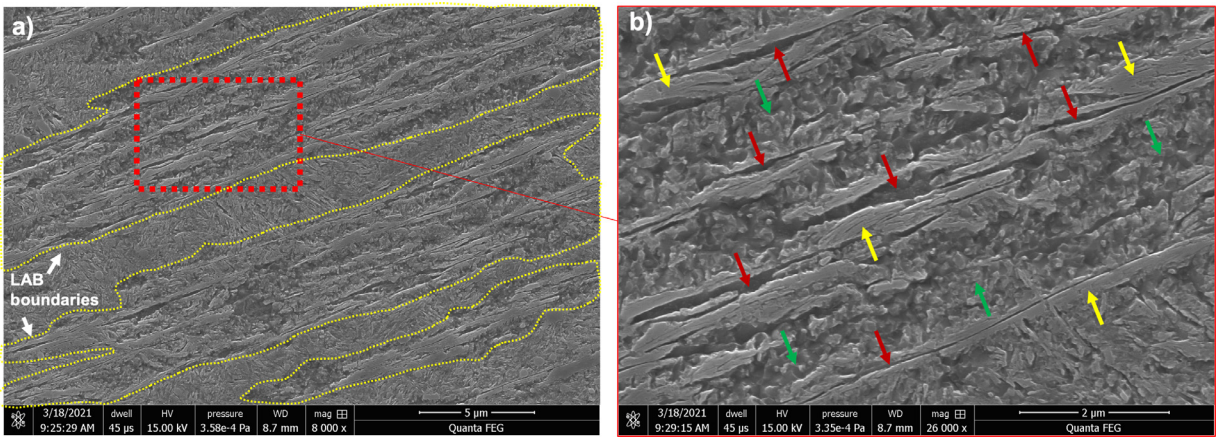

Fig. 4. a) Thick late-stage LAB from sample under 2.9 GPa for 1116 million cycles with LAB boundaries highlighted in dash lines. b) Higher magnification of late stage LAB showing all three LAB constituents. Red arrows indicate elongated grains, yellow arrows indicate lenticular carbides and green arrows are equiaxed grains.

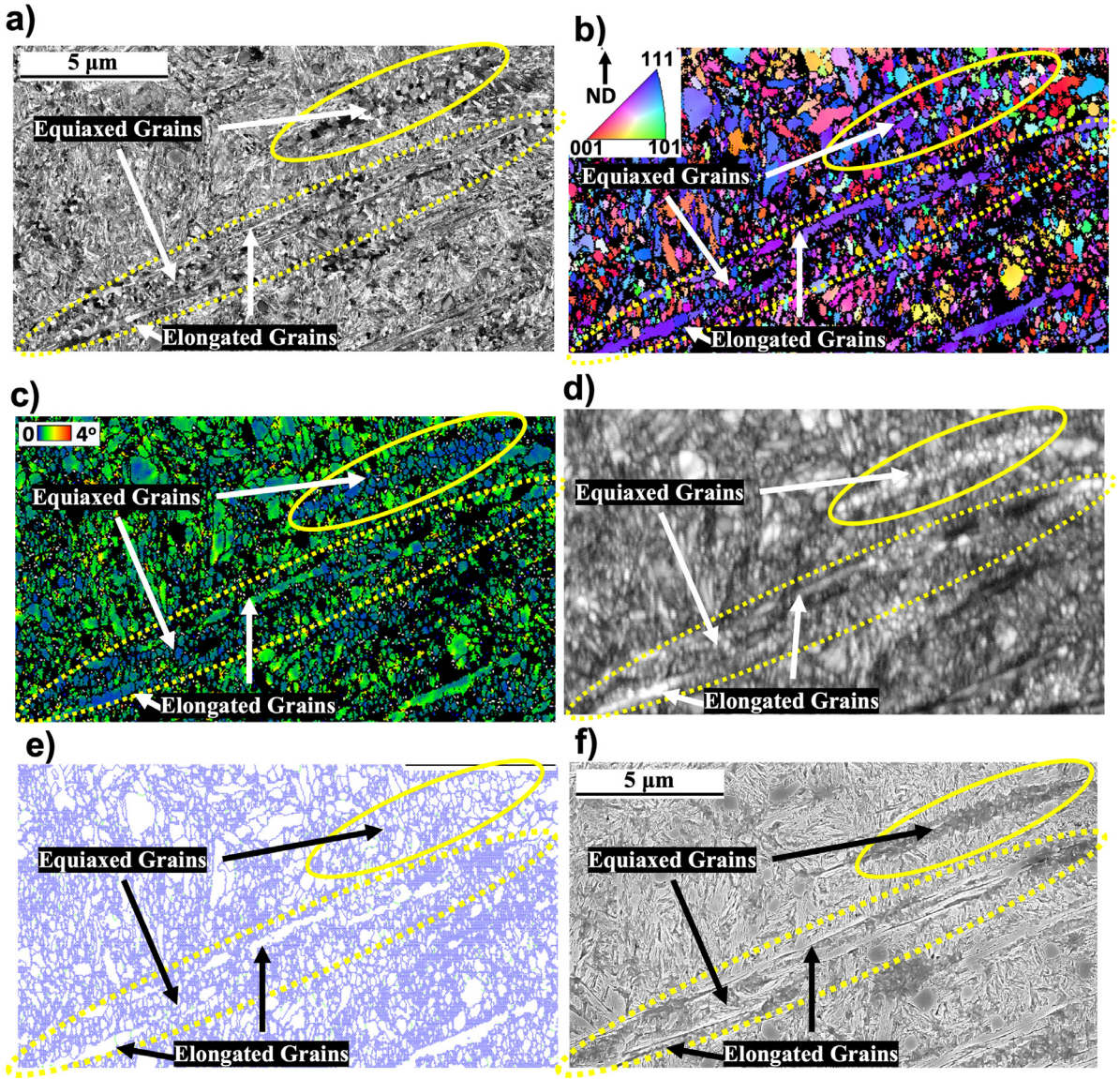

Fig. 5. Images of LAB in a bearing sample tested under 2.9 GPa for 3016 million cycles. a) BSE SEM image b) IPF map (bcc, CI>0.1) c) KAM map (100nm,5°) (bcc, CI>0.1) d) IQ map of region e) HAGB map (blue line indicate grain boundaries with misorientations ≥ 15°) and f) SE SEM image. Solid circle highlights an early stage LAB consisting of only equiaxed grains while the dashed circle highlights a late-stage LAB consisting of both equiaxed and elongated grains. Lenticular carbides remain unindexed in the EBSD maps and hence appears black adjacent to the elongated grains in EBSD maps.

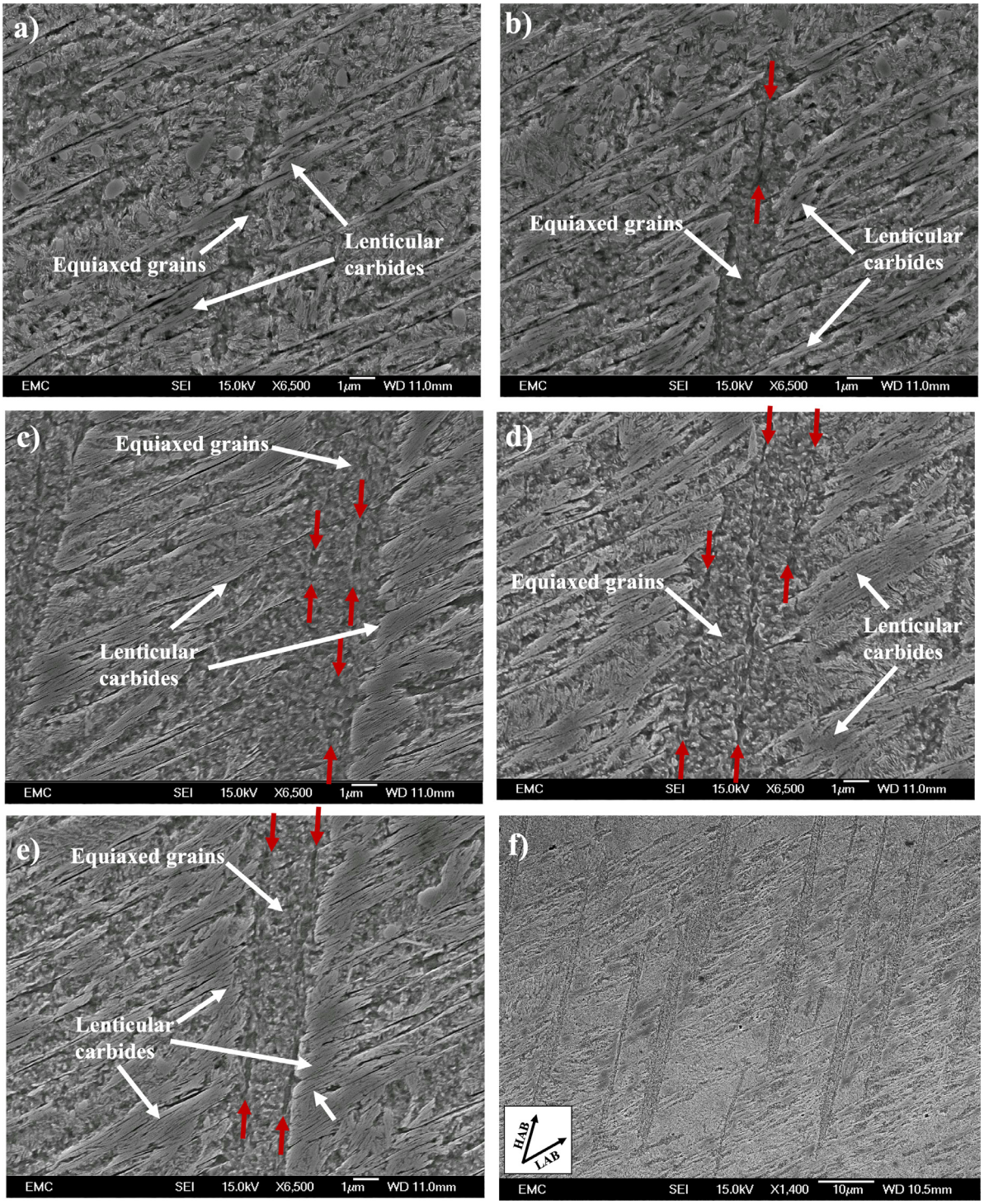

Fig. 6. SEM images of different development stages of HAB from bearing samples tested under 2.9 GPa for a) 1116, b)1338, c&d&e) 3016 million cycles showing the evolution of HAB from early (a) to intermediate (b) and late (c&d&e) stages. Area showing mixture of multiple fully developed LAB and HAB from bearing sample run under 2.9 GPa for 4141 million cycles is shown in f). Red arrows show the elongated grains within the HAB.

in section 3.3, Fig. 7f shows an SE SEM image of the surface after being etched. It is difficult to differentiate the elongated grains from the equiaxed grains in the BSE image shown in Fig. 7a, however they are easily differentiated in the KAM, IQ, IPF and HAGB maps shown in Figs. 7b-e). The grain boundaries in the HAGB map (Fig. 7e) clearly show a difference in grain structure between the elongated ferrite grains and the surrounding equiaxed grains in the HAB where the former is much larger in size and has the long axis parallel to the band orientation (~30° for LAB and ~80° for HAB). Also, the equiaxed grains in the HAB have shown to have relatively low misorientation compared to the elongated grains and surrounding microstructure (Fig. 7c). Equiaxed grains also show a relatively high IQ contrast evidenced by the higher brightness compared with the surrounding microstructures except the elongated grains (Fig. 7d). Areas with high IQ contrast (brighter appearance) are regions with relatively low local strain thus low dislocation

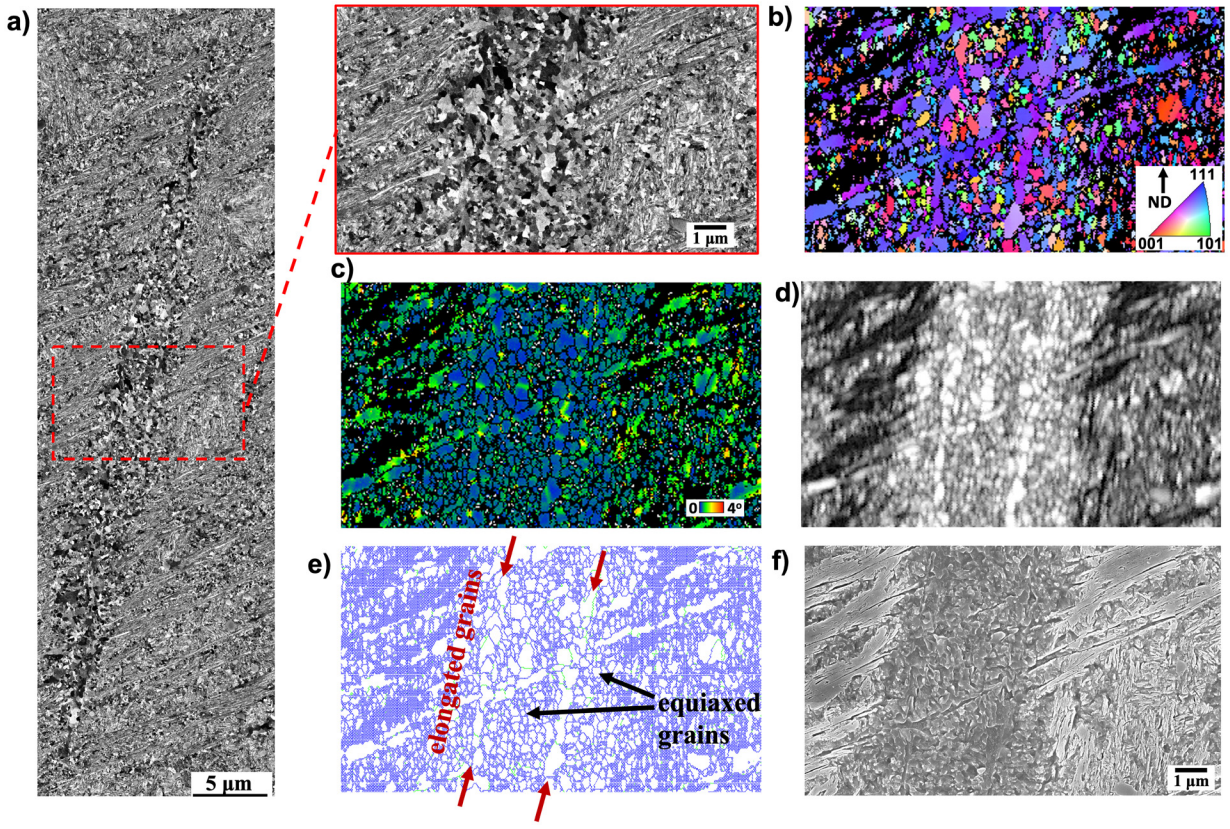

Fig. 7. HAB in a bearing sample tested under 2.9 GPa for 3016 million cycles shown as a) BSE SEM image and EBSD maps of highlighted area of HAB in a) shown as b) IPF map (bcc, CI>0.1) showing directions parallel to normal direction c) KAM map (100nm,5°) (bcc, CI>0.1) d) IQ Map e) HAGB map (blue line indicates grain boundaries with misorientations ≥ 15°) and f) SE SEM image.

density and defects, which is a typical outcome of recrystallization in deformed materials responding to a build-up of stored energy [18]. Ferrite phases typically have lower internal strains compared to martensite [19], hence show a higher IQ contrast. This provides the evidence supporting the hypothesis that equiaxed grains (in LAB and HAB) are ferritic and are formed likely due to recrystallization [10]. From Fig. 7b, a general alignment of the grain structure with a <111> axis that is approximately parallel to the normal direction (ND), particularly the elongated grains, is seen similar to LAB. Also, the equiaxed grains appear to have a larger variation in grain orientations comparing with the elongated grains (Fig. 7b).

Fig. 8 presents SEM images of a different HAB observed in the same sample (2.9 GPa 3016 million cycles), showing a fully formed elongated grain of about 8 µm in length within the HAB comparing with those at much early stages in Fig. 7. Fig. 8b shows that the elongated grain has a more distinct texture (uniform colour in IPF map) and is much bigger comparing with the surrounding equiaxed grains which range from 100–300 nm in size with various grain orientations (based on those shown in Fig. 7 and Fig. 8). Comparing the structures of the elongated grains in the two HAB shown in Figs. 7b and 8b, elongated grains in Fig. 7 at early stage consist of multiple coarse grains surrounded by finer equiaxed grains with various grain orientations, while that in Fig. 8 at a late stage, consists of one large elongated grain in a more uniformed orientation. This suggests elongated grains form from equiaxed grains through a grain rotation and coalescence process. The fully developed elongated grain also shows to have a build-up of misorientation (Fig. 8d) as the green scale becomes more dominant across the grain that is likely due to deformation arising from shearing effect through the plastic deformation of the newly formed coarse grain.

3.5. Nano-hardness of the microstructural alterations

To confirm and compare the properties of the different microstructural components in WEB, two types of nano-indentation measurements have been performed.

The first one was performed on a WEB area with an array of 30 × 35 indents at 1 μm spacing between two adjacent indents on an unetched surface from a bearing sample tested under 2.9 GPa for 4141 million cycles. After hardness test, the surface was then etched and imaged using SEM (Fig. 9a) to compare the position of the microstructural features with the hardness color map generated from the indentation matrix in Fig. 9b. It clearly shows that the ferrite bands, in the HAB, have a lower hardness than that of the parent martensite matrix and the lenticular carbides, with the latter being much harder than the steel matrix. The lenticular carbides were found to have a similar hardness to spherical primary carbides seen at the top of Fig. 9. Furthermore, the softest regions within the bands is shown to correspond to the position of the elongated grains in Fig. 9b possibly due to grain coarsening as observed from the EBSD results.

A second nano-hardness test was then conducted on a WEB area with an indent matrix of 10 × 46 at a spacing of 3 μm between adjacent indents. After indentation, the surface was imaged with SEM to determine the exact location of each indent, it was then etched to identify the microstructural features and again imaged with SEM. The two SEM images were then overlayed and the

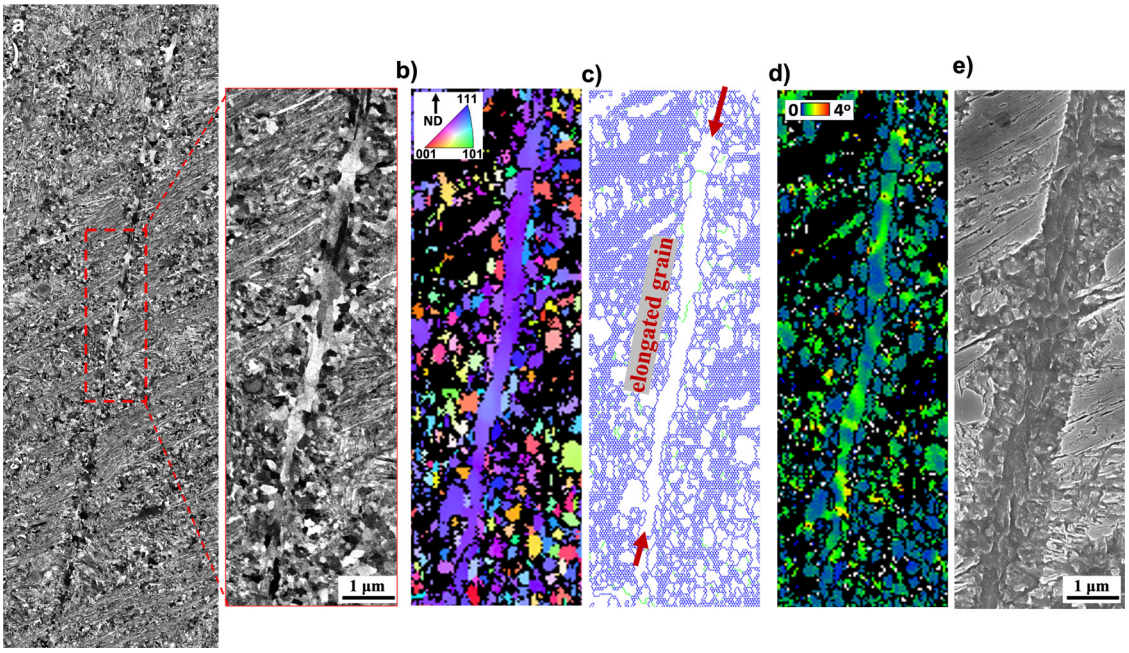

Fig. 8. SEM images of a larger HAB in the bearing sample tested under 2.9 GPa for 3016 million cycles. a) BSE SEM image b) IPF map (bcc, CI>0.1) showing directions parallel to normal direction c) HABG map (blue line indicate grain boundaries with misorientations ≥ 15°) d) KAM map (100nm,5°) (bcc, CI>0.1) and e) SE SEM image.

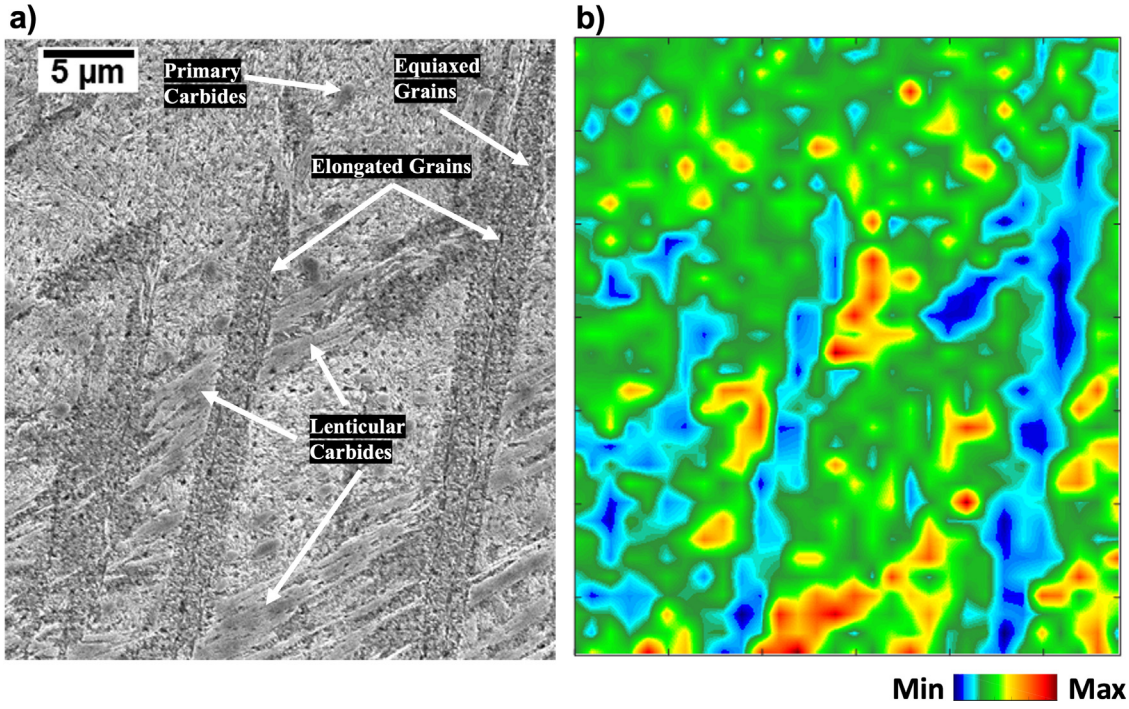

Fig. 9. a) An SEM image of an area in the subsurface of a bearing tested under 2.9 GPa for 4141 million cycles, showing LAB and HAB features. b) A hardness color map from a nano-indentation test on an area with LAB and HAB features shown in a) to indicate significant changes in hardness.

indents were categorized into each of the microstructural features observed (see an SEM image showing locations of the indent in the WEB in Fig. 10). The penetration depth of the indentation was kept at 50 nm to provide indents small enough to be fully positioned within each constituent of the WEB. Only the hardness measurements from indents that are fully embedded within a feature have been used to calculate the average hardness of that feature. The analysis of these micro-features at this scale makes it possible to determine the hardness of equiaxed ferrite grains, elongated ferrite grains and the lenticular carbides in WEB at the highest precision. The 'indents' on the SEM map were graphically added on the SEM map of the etched surface after indentation to show the position of each indent clearly and the corresponding microstructural features. A minimum of 10 measurements from each constituent have been used and the averaged hardness values are shown in Table 3, and

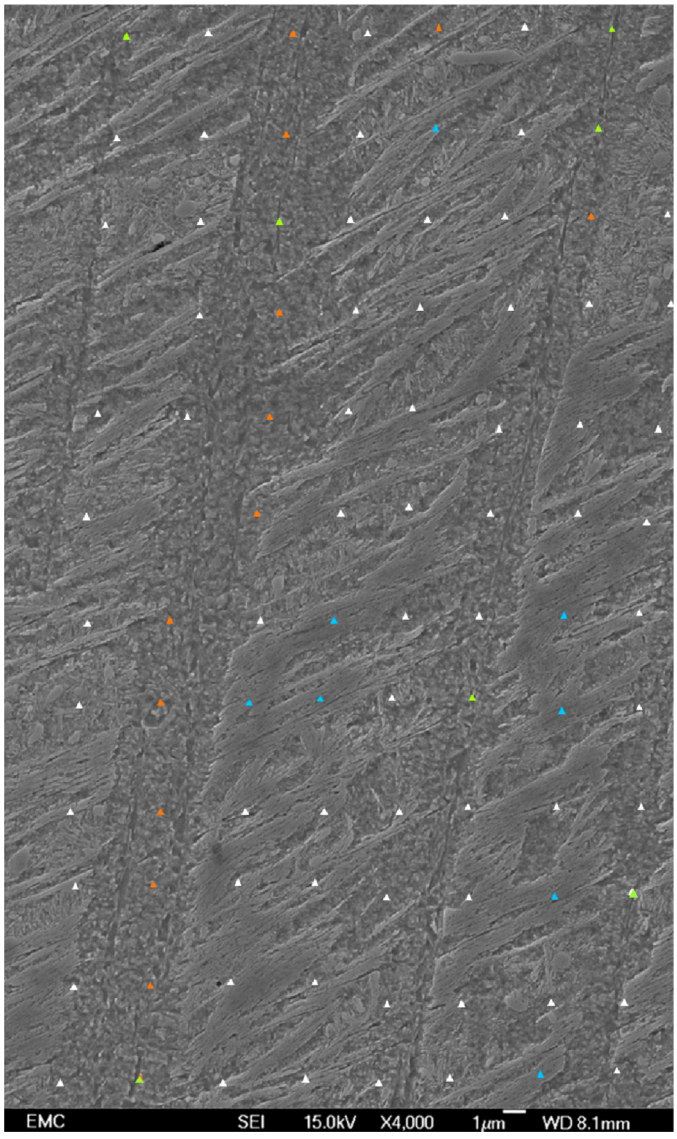

Fig. 10. An SEM image of the etched surface post the nano-indentation test with 3 μm spacing and 50 nm indent depth on a bearing sample tested under 2.9 GPa for 4141 million cycles. Orange, blue and green triangles indicate positions of the indents in equiaxed ferrite grains, lenticular carbides and elongated grains respectively.

Table 3
A summary of the averaged nano-hardness values and their standard deviations for the three WEB constituents and the parent steel matrix.

	Hardness (GPa)
Equiaxed grains	**5.04 ± 0.8**
Elongated grains	**4.40 ± 1.1**
Lenticular carbides	**9.67 ± 1.9**
Parent Matrix	**7.1 ± 1.9**

the hardness follows: lenticular carbides > martensite > equiaxed grains > elongated grains.

3.6. Interfacial energy of lenticular carbides during LAB to HAB transition

To investigate the drivers of the transition from LAB to HAB, interfacial energy of lenticular carbides in LAB and HAB both under fully developed conditions are compared. Carbide dissolution has been found to be driven by significant energy build-up that eventually destabilises carbides [20–22]. The free energy build-up driving carbide dissolution could arise from i) interfacial energy, ii) difference in binding energy between C-Fe in the carbide and C-dislocation and, iii) elastic energy increase in heavily dislocated regions [20].

The interfacial energy of the carbides ($E_{LC\alpha}$) can be determined from Eq. 1 [23], where γ is the specific interfacial energy between ferrite and carbide, V_m is the molar volume of the cementite and $\frac{dSA}{dV}$ is the ratio between the surface area of carbide/ferrite and the volume of the carbides. According to this equation, the change in interfacial energy of carbides is proportional to the surface area to volume ratio of the carbides. Hence the comparison between the surface-volume ratios of the lenticular carbides in a dense LAB region and a HAB region can provide an insight to the interfacial energy for the two features.

To achieve this, SEM images of fully developed (late-stage) LAB and HAB (area of 11 × 15 μm) have been selected for the comparison as shown in Fig. 11a and Fig. 11d respectively. Given that HAB develops later in dense LAB regions, it is assumed the LAB area in Fig. 11a would transition to an HAB area similar to that shown in Fig. 11d had the RCF-test been run for longer. A mask is applied on the original SEM images (Fig. 11a and Fig. 11d) to highlight the carbides in both LAB and HAB, as shown in Fig. 11b and 11e respectively. By vertically (into the page) extending the highlighted carbide areas in Fig. 11b and Fig. 11e by a depth of 44 μm (the average depth of developed LAB [3]), a 3D model of the carbides is created for the LAB (Fig. 11c) and HAB (Fig. 11f). The volume of the carbides in 3D images has then been used to determine the $\frac{dSA}{dV}$ of the lenticular carbides for both cases. ImageJ is used in the 3D model construction and the measurement of the surface area and volume of the carbides. The results are summarised in Table 4.

$$E_{LC\alpha} = \gamma \,.\, V_m \,.\, \frac{dSA}{dV} \tag{1}$$

A significant reduction in $\frac{dSA}{dV}$ of approximately 6 times is seen during the transition from LAB to HAB. This suggests that the continuous growth of LCs and free-energy build-up during the LAB development has eventually destabilised the structure and led to the transition to a lower surface energy structure of HAB. Hence is suggested that the interfacial energy of LCs is the driver for LC breakdown in LAB and transition from LAB to HAB. Hence the LAB to HAB transition can be described as a form of energy release in the microstructure.

4. Discussions

This study has confirmed that WEB (both LAB and HAB) consist of three main constituents equiaxed grains, elongated grains and lenticular carbides tas it has been observed in the recent study [10]. It has also revealed that LAB and HAB development follow similar stages and mechanisms although at different scales.

The first stage of microstructural alteration in the formation of LAB is found to be the formation of very small bands of equiaxed ferrite grains (Fig. 2). Over the increase of stress cycles during this stage, the bands grow in both thickness and length to up to 1-2 μm width and 10 μm in length. EBSD analysis has shown these bands have a higher IQ contrast compared to the surrounding matrix, suggesting a lower number of defects, such as strains and dislocations, in the bands and ferrite regions [19]. Coupled with the relatively low misorientation of the equiaxed grains shown in the KAM maps, this provides a strong evidence that these grains are ferritic and likely formed due to recrystallization.

Nucleation sites of recrystallized grains arise in regions of microstructure with relatively high dislocations. Recrystallisation oc-

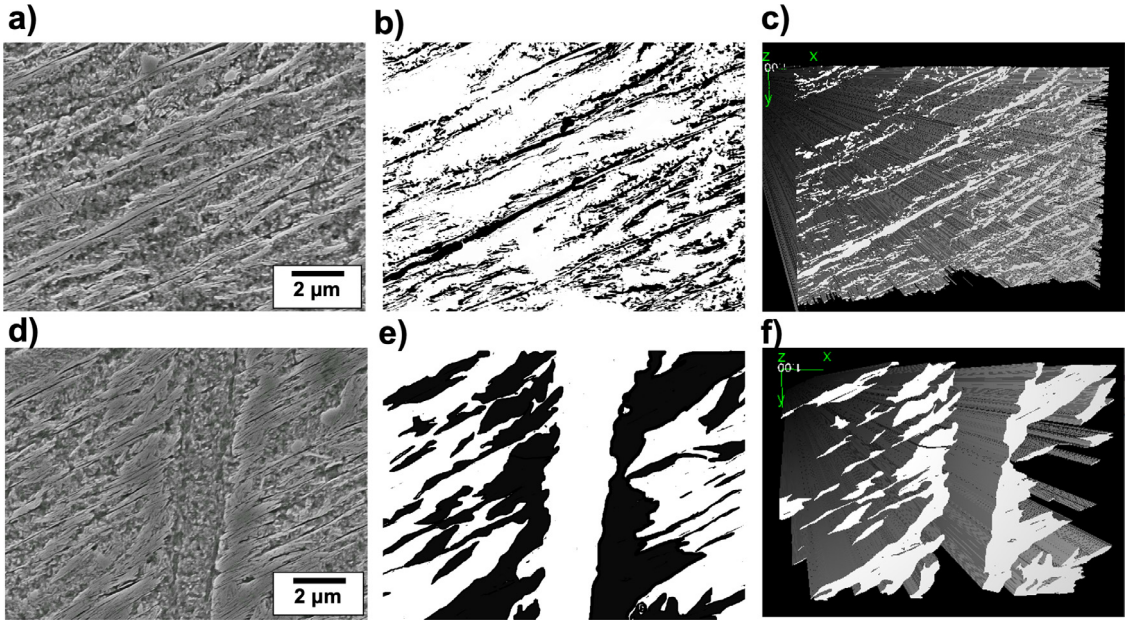

Fig. 11. Images of LAB (a-c) and HAB (d-f) in a bearing sample tested under 2.9 GPa for 3016 million cycles. a&d) SEM images, b&e) after mask is applied to a&b, highlighting the carbides in the area, c&f) re-constructed 3D images of b&e, showing carbides in the area (average depth of 44 μm is applied).

Table 4
A summary of the volume and surface area measurements of LCs in the LAB and HAB shown in Figure 11

	LCs associated with LAB	LCs associated with HAB
Volume (μm^3)	**4,994**	**5,376**
Surface Area (μm^2)	**203,003**	**34,588**
Surface Area / Volume Ratio $\frac{dSA}{dV}$ (μm^{-1})	**40.65**	**6.43**

curs as a way of releasing the energy built-up due to local plastic deformation. According to the observations of LAB being developed within DERs [2,6], there might be a significant energy build-up within DER that leads to this recrystallization process during LAB formation. For the cases where LAB form without DER in softer steels (hardness lower than 720 HV) [11,12], it suggests that in softer steels, energy build-up must have occurred in the microstructure at much earlier stage without the need of DER formation, which has been reported to be a 'softening' process [1]. Hence, an initial energy build-up in the microstructure may be the driver of LAB initiation or first recrystallisation. While the formation of stressed points in the microstructure leading to the first recrystallisation (LAB nucleation) remains unclear, the nucleation of HAB during the second recrystallization stage is believed to be correlated with the lenticular carbides destabilisation in LAB. This has been demonstrated by the substantial interfacial energy reduction during the transition from LAB to HAB. It has also shown that the equiaxed grains in LAB cause breakdown of pre-existing microstructure such as primary carbides within the bands (as shown in Fig. 2e).

Various studies have investigated the influence of plastic deformation on cementite dissolution in steel microstructures and the factors influencing the stability of the carbides. The driving force for carbide dissolution in the microstructure is the supply of energy that is sufficient to destabilise the carbide. The energy could arise from the interfacial energy that increases the Gibbs free energy of the carbide [20]. The interfacial energy is heavily dependent on the surface area to volume ratio $\frac{dSA}{dV}$ of the carbide. Shapes with a low $\frac{dSA}{dV}$ demonstrate a lower interfacial energy and greater stability, which explains why primary carbides are typically spherical. As shown in Table 4, the thin and long and densely packed lenticular carbides in the late stage LAB have a much higher $\frac{dSA}{dV}$ ratio (6 times) comparing that of the lenticular carbides surrounding HAB, thus the transition from LAB to HAB would make the carbides much more stable structures. It has also been reported that ferrite/carbide interfaces are preferential sites for dislocation pile-up, causing an increase in the interaction energy which can exceed the binding energy of C-Fe leading to the break of C-Fe bonds in carbides [21,22], hence the subsequent recrystallisation (HAB nucleation) is a way of reducing the overall energy in the system due to the build-up of dislocation pile-ups at the ferrite/carbide boundary in LAB. This also explains why HAB initiates from the dense region of LAB [3,13].

The developed equiaxed ferrite grains either in the LAB or the HAB appear to later transform towards elongated grains which have a preferential orientation close to a <111> direction // ND which is similar to a previous study [10] and typically observed in cold rolled steel. However, during the early stages, elongated ferrite grains appear as small slightly distorted individual grains that are coarser than the surrounding equiaxed grains (Fig. 7) showing little variation in their orientations. Later, multiple grains started to align and elongate at approximately 80° to the rolling direction (see in Fig. 8), showing coalescence of the individual grains into a longer elongated grain within the HAB. Based on the grain structures shown in Fig. 5, a similar process is proposed in the LAB. During this process, grain rotation/coalescence appears to have occurred. Similar process has been reported in nanocrystalline metals when plastic deformation results in texture development through rotation of adjacent grains across preferential slip systems and eventually leads to coalescence as a form of grain growth (illustrated in Fig. 12) [24–28]. Within the grain pair, due to plastic deformation one grain rotates to align with the adjacent grain result-

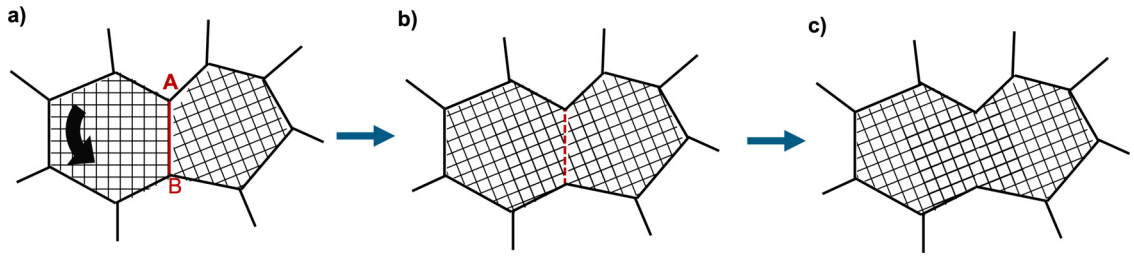

Fig. 12. An illustration of the grain rotation and coalescence theory due to plastic deformation in nanocrystalline materials, showing a) rotation of one of two adjacent grains with a high-angle grain boundary. b) The high-angle grain boundary become a low-angle grain boundary after the grain rotation c) fully coalesced grains resulting in a coarser and elongated grain. Figure adapted from [24].

ing in the reduction of the initial high-angle grain boundary AB in Fig. 12a to a low angle grain boundary in Fig. 12b and the grains eventually coalescence as shown in Fig. 12c through the elimination of the adjacent grain boundary between the two grains. This is believed to be a form of recovery in the microstructure driven by the reduction of the boundary energy of the system [24,28]. This explains the formation of the elongated grains shown in Fig. 7, where the initial individual grains coarser than the equiaxed grains with a similar grain orientation (after rotation) have grown (coalesce) into longer grains (the elongated grains) as shown in Fig. 8. Within the ~8 μm elongated grain, some low-angle grain boundaries are still visible (green lines in Fig. 8c) suggesting a possible transition from high-to-low angle grain boundaries and eventually fully coalescence. It has been previously proposed that the elongated grains in both LAB and HAB show a <111>{112} slip system aligned with the long axis of both bands (30° and 80° to the rolling direction respectively) [10], which agrees with the findings from this study that plastic deformation of the equiaxed regions in WEB occurs through grain rotation towards preferential slip systems that are likely aligned with the shearing component responsible for the LAB and HAB orientations. The alignment of grains results is a form of recovery through the elimination of common grain boundaries and grain growth thus the formation of elongated grains. The proposed alignment of the elongated grains with a shear component is based on the higher deformation observed compared to the surrounding more randomly orientated equiaxed grains (see KAM maps in Figs. 5c, 7c and 8d). Modelling of uniaxial testing conducted by Chen et al. [39] has shown that activation of slip systems conforms with the highest Schmid factor in each grain which is influenced by the grain orientation. Given that the elongated grains with an established texture are more deformed (based on KAM maps) compared to the surrounding equiaxed grains which have more heterogeneous orientations suggests a maximum Schmid factor associated with the LAB and HAB orientations. However, modelling of the local microstructure prior to LAB and HAB formation (including closely-packed carbides) would be required to further investigate this.

The coarse grains of the elongated grains are also evidenced from the nano-indentation analysis, where they show to have a lower hardness comparing with the surrounding equiaxed grains. The overall hardness of the LAB and HAB is lower than that of the martensitic parent matrix, suggesting that they are ferritic structures. Hardness values of equiaxed grains and lenticular carbide in WEB reported by Smelova et al. [10] being 4.2–6 GPa and 9–11 GPa respectively are similar to those obtained in this study (5.04 ± 0.8 GPa and 9.67 ± 1.9 GPa respectively), however a much smaller indentation size has been used in this study to ensure that the indent falls well within an individual feature, e.g. equiaxed and elongated grains, without overlapping the neighboring microstructures. Previous hardness tests, as discussed by the authors [10], used an indent size which was comparable to some of the features that has caused some uncertainty in their measurements. This is addressed in this study by using an indent size smaller that the size of the features. It is also interesting to see that the primary carbides have a similar hardness to the lenticular carbides (shown in Fig. 9) or carbon-rich areas as reported in [10]. Nonetheless, further investigation is required to compare primary carbides in the microstructure with lenticular carbides in LAB.

5. Proposed formation and evolution mechanism of LAB and HAB

5.1. LAB formation mechanisms

Based on the characteristics of LAB found in SEM analysis using a range of techniques, the evolution of the LAB has been defined as three stages. The initial or early stage of LAB is characterized by the formation of equiaxed ferrite grains as a band that grows in length and thickness (Fig. 13a and 13b). This is followed by the formation of elongated ferrite grains within the equiaxed grain band (Fig. 13c) accompanied by lenticular carbide formation adjacent to the elongated grains. The growth of both the elongated ferrite grains and the lenticular carbides across the equiaxed ferrite grain band results in the commonly observed ‘cotton-bud’ shape shown in Fig. 13d. This cotton-bud shape has a ‘head’ consisting of equiaxed grain and the ‘stem’ section of the shape consisting of elongated ferrite grains and lenticular carbides. For larger equiaxed ferrite grain bands, multiple elongated grains surrounded by lenticular carbides may develop within the band parallel to each other which is considered the late stage of LAB (Fig. 13e).

Most past literature have suggested that lenticular carbides nucleate at the edges of the equiaxed grained LAB [9,29,15,30,5] [31-33,14,34], which is unfortunate against the SEM evidence obtained from this study. As shown above, lenticular carbides originate at the edges of elongated ferrite grains and developed within the equiaxed grains of the LAB rather than at the edges of the LAB equiaxed grain region.

A possible explanation for the nucleation of the lenticular carbides at these sites is by the grain rotation-coalescence theory discussed above. APT analysis of white-etching matter such as WECs and WEAs have shown that in equiaxed ferrite grains, the carbon is typically segregated at the grain boundaries rather than inside the grain due to the incompatibility of the carbon with the ferrite matrix [35,36]. Assuming a similar arrangement in the equiaxed ferrite grains of LAB, carbon would also be segregated at the grain boundaries. Hence during the transformation of equiaxed to elongated ferrite grains as a form of recovery, the elimination of adjacent grain boundaries during coalescence would release the segregated carbon atoms leading to a diffusion of carbon towards the grain boundaries of the newly formed elongated ferrite grain which would have a higher carbon concentration compared to the carbon concentration in the grain boundaries of the initial equiaxed grains. Thus it becomes possible that lenticular carbides nucleate at the edge of the elongated grains once enough carbon

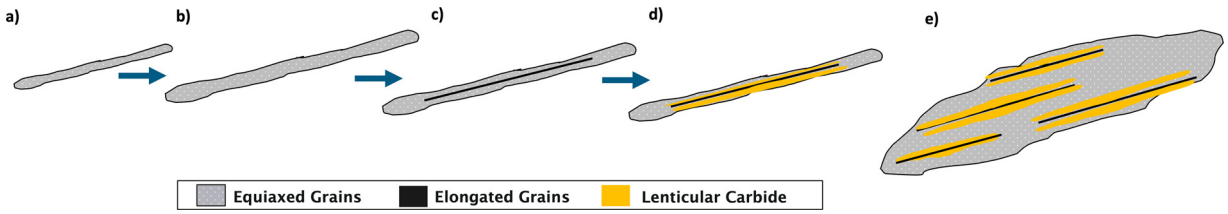

Fig. 13. A schematic showing LAB evolution from the initial stage as a small band consisting equiaxed grain (a) growing in length and thickness (b). During the intermediate stage (c), elongated grains develop within the equiaxed grained band and eventually lenticular carbides nucleate at the edge of the elongated grains and grows leading to the cotton-bud shape shown in (d). At the latest stage, LAB multiplies forming dense LAB areas showing in (e).

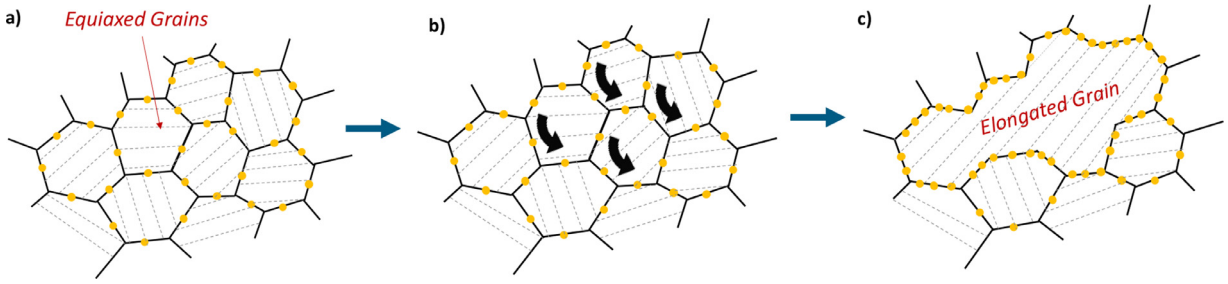

Fig. 14. A schematic of the formation of elongated grains and lenticular carbides in LAB. a) Equiaxed grains of various orientations in LAB with carbon segregated at grain boundaries. b) Grain rotation and coalescence in LAB leading to formation of elongated grains. c) A fully developed elongated grain where carbon in the elongated grain boundaries due to coalescence have migrated to the boundaries of the elongated grains leading to nucleation of lenticular carbides. Yellow marks indicate carbon.

has accumulated during coalescence. The carbon diffusion in this instance may be driven by dislocation-assisted carbon diffusion or free carbon diffusion as it was suggested in [9].

Due to the much shorter distance that carbon atoms actually travel, about 50 – 300 nm as opposed to the literature suggested 9 µm [29], it is thus understandable that the theoretical models in literature provide a much later LAB initiation prediction [9,29,14,15,37] than that from this study [13]. This has been further demonstrated by the formation of multiple elongated grain-LCs structures during the late stages of LAB development. However, the lenticular carbides could grow much thicker than that of elongated ferrite grains, suggesting that the nucleated carbides also act as carbon sinks driving the carbon in surrounding equiaxed ferrite grains to migrate to the LCs (likely due to dislocation-assisted diffusion [9]). It is therefore important to differentiate between the nucleation stage of the lenticular carbide (where free carbon diffusion plays a role) and the growth of the carbide after nucleation due to dislocation-assisted diffusion. A schematic of the formation of elongated grains and lenticular carbides in LAB is shown in Fig. 14.

5.2. HAB formation mechanisms

Looking at the HAB which form later in the bearing life, characteristics similar to LAB are observed, e.g. starting from the formation of equiaxed ferrite grains (Fig. 6a) followed by the formation of elongated grains within the equiaxed grain region (Fig. 6b-e) and then lenticular carbides growing at the edges of HAB equiaxed grain region instead of adjacent to elongated grains. A schematic of the HAB formation stages is shown in Fig. 15. The high IQ contrast and low misorientation of equiaxed grains (Fig. 7) suggests they are products of recrystallization similar to that in LAB. As HAB grows, the pre-existing LAB features such as lenticular carbides dissolve within the newly formed HAB and the LCs at the edges of HAB act as carbon sinks for carbon inside the HAB to migrate to the edges (Fig. 7c-e). As discussed above, the driver of equiaxed grains formation in HAB (initial stage HAB) is most likely the high interfacial energy of the close-packed lenticular carbides in late stage LAB, which leads to an energy build-up locally to be released via recrystallization to break down the lenticular carbides. At the early-stage of LAB, when they are scattered single bands, the energy build-up across individual lenticular carbides is insignificant, which later becomes significant and drives the formation of HAB due to the growth in size of LCs and formation of dense closely packed LAB. The energy build-up in LAB is thus the driver for HAB initiation through recrystallization where LCs break down to more stable geometries releasing the stored energy in the region. The dissolution of the pre-existing lenticular carbides in LAB within the HAB results in free carbon releasing and migrating to the carbides outside the HAB (see Fig. 15e) causing LC thickening at the HAB boundaries. This suggests that the LCs act as carbon sinks that also attract carbon from the equiaxed grains to the carbide given the incompatibility of carbon in the ferrite matrix of the band. The much lower interfacial energy of the LCs in HAB comparing that of the LAB, (see their surface-volume ratios in Table 4) suggests that a second stage recrystallization takes place during HAB formation.

As mentioned above, the major difference between HAB and LAB is that no new lenticular carbides develop adjacent to the elongated grains of the HAB. This could be explained by difference in the surrounding microstructures of LAB and HAB during their initiation. For LAB, it is seen in Fig. 2e that primary carbides (circled in green) in the path of the equiaxed ferrite bands dissolve which likely results in carbon accumulation within the bands. This is an expected observation during recrystallization where pre-existing features breakdown during the formation of new grains. This suggests that pre-existing features such as primary carbides, tempered carbides or even the martensitic matrix all of which typically have a relatively higher carbon content dissolve within the equiaxed grains of the band leading to carbon build-up in the LAB. Once the elongated grains develop, lenticular carbides nucleate which then acts as carbon sinks to reduce the carbon accumulation within the band [9]. Prior to the nucleation of the lenticular carbide with the elongated grains, there are no obvious carbon sinks leading to the carbon saturation of the band.

Another important element in this is the role of dislocations, i.e. how they contribute to the nucleation and growth of lenticular carbides and their eventual dissolution during HAB formation. In LAB, lenticular carbides nucleate at the edges of elon-

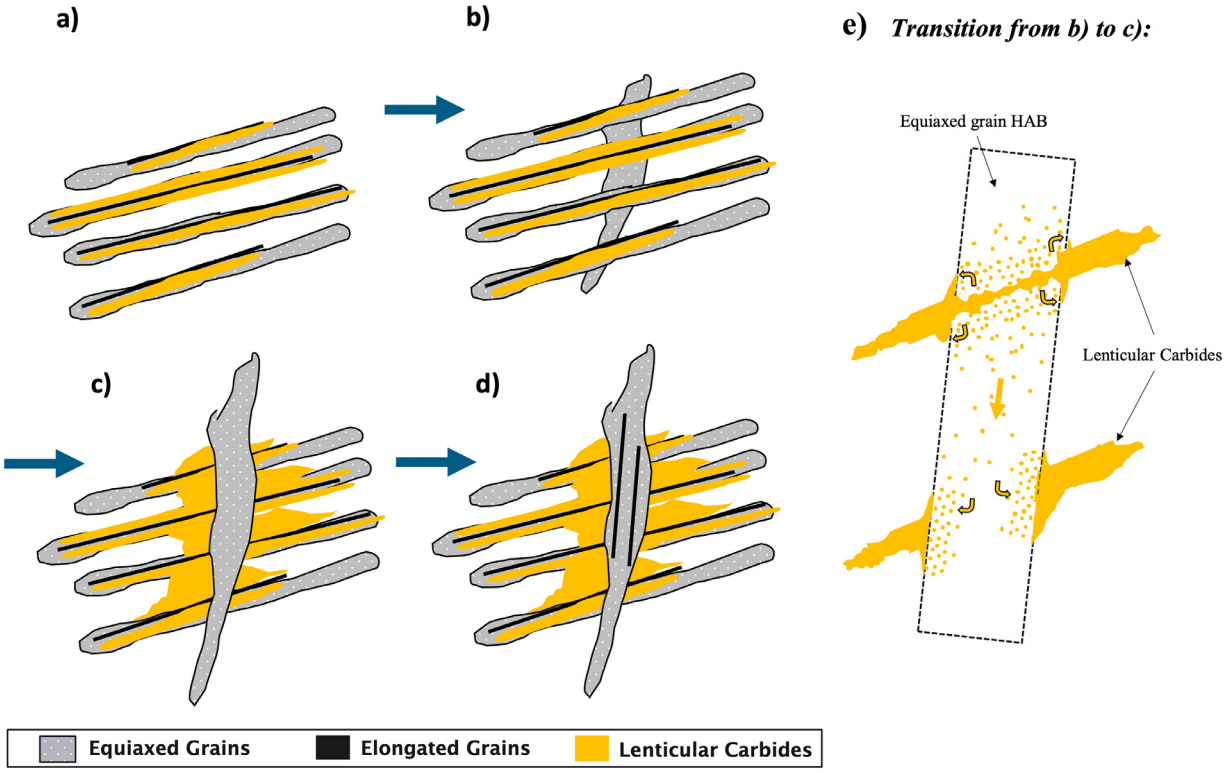

Fig. 15. A schematic showing the HAB evolution process starting from a) dense LAB region b) equiaxed HAB forming in region with dense close-packed LAB c) breakdown of pre-existing features such as lenticular carbides within the HAB and the carbides thicken/merge at the HAB edge making clear boundary. d) Elongated grains develop gradually within the equiaxed grains of HAB. e) The breakdown of lenticular carbides within HAB (transition from b-c) where the resulting free carbon in the HAB later migrates to remaining lenticular carbides at the edge which act as carbon sinks and the HAB becomes a sort of diffusion channel. Arrows indicate the direction of migration of excess free carbon in the band.

gated grains during their formation through rotation/coalescence of equiaxed grains, where gradual elimination of common boundaries releases the initially segregated carbon, leading to carbon migration to newly formed grain boundaries of the elongated grains through dislocation-assisted migration [9] or free carbon diffusion which is possible due to the small diffusion distance of 50-300 nm discussed previously. Initially, it would be the dislocation-assisted carbon migration that leads to the thickening of carbides as well as pile-up of dislocations at carbide interface. As lenticular carbides grow, its $\frac{dSA}{dV}$ increases, leading to a build-up of dislocations at its edge and increase in interfacial energy until it is higher than the binding energy of C-Fe, leading to their dissolution that initiates HAB.

The initial carbon build-up in the equiaxed grains in a HAB is likely to originate from the breakdown of lenticular carbides within the band. However, at the early formation stage, HAB are surrounded by multiple LAB (consisting of multiple lenticular carbides) which can attract carbon from the equiaxed grains of the HAB prior to the formation of elongated ferrite grains due to deformation. This is evidenced from Fig. 6 where continuous thickening of the lenticular carbides at the edges of the HAB (see schematic in Fig. 15b-c and 15e). Hence when the elongated grains develop (see Fig. 15d), there is no significant carbon available any more to accumulate at the edges of the newly formed elongated grains. An earlier study has suggested through microprobe analysis that HAB have a lower carbon content compared to LAB which would support the theory that there is less carbon accumulation in the HAB equiaxed grains than the LAB equiaxed grains when the elongated grains develop [6,38].

6. Conclusion

This study has analysed both LAB and HAB formed in ACBBs using SEM, EBSD and nanoindentation techniques. Detailed analysis has provided evidence of the three main constituents in LAB and HAB being equiaxed grains, elongated grains and lenticular carbides. The samples tested at a range of stress cycles have enable the elucidating of LAB and HAB evolution mechanisms. A formation mechanism theory is thus proposed based on the experimental findings.

- LAB form in three stages: at the early stage, bands of equiaxed ferrite grains develop within the maximum shear stress region. As the equiaxed ferrite band grows in length and thickness, the intermediate stage shows elongated ferrite grains developing within these bands due to plastic deformation with lenticular carbides nucleating at the edge of the elongated grains. These carbides grow in thickness across the equiaxed ferrite grains of the LAB. At late-stage multiple densely packed bands merge together leading to large regions of LAB fully consuming the parent microstructure.
- HAB is observed initially as a band of equiaxed ferrite grains developing within regions of dense late stage LAB where pre-existing features such as the LAB constituents (elongated grains, lenticular carbides) gradually breakdown as the equiaxed HAB grows in length and thickness. Later stages of the HAB show elongated grains later develop within the equiaxed bands similar to LAB. In late stages, lenticular carbides at the edges of the HAB continue to thicken and merge together creating clear boundaries between the HAB and the remaining lenticular car-

bides surrounding the HAB. Unlike LAB, no new lenticular carbides develop parallel to the HAB.

- The formation of equiaxed ferrite grains in both LAB and HAB is most likely a result of recrystallization to release the energy-build-up in the system during operation. Fully developed lenticular carbides during LAB formation show an unstable structure with a high surface-volume ratio. The build-up of closely packed lenticular carbides in high LAB density regions leads to local energy-build up in the microstructure which is released through a recrystallization stage (HAB formation) which breaks down the lenticular carbides into more stable geometries by reducing the interfacial energy of the carbides. A similar energy build up in the initial microstructure is believed to contribute to the initiation of the LAB recrystallization stage.
- The formation of elongated grains within the recrystalized equiaxed ferrite grains in LAB and HAB is a form of recovery due to plastic deformation induced grain rotation and coalescence driven by the reduction of the overall grain boundary. In LAB, this occurs in carbon-saturated equiaxed grains, hence the elimination of grain boundaries results in the release of carbon and its accumulation at the grain boundaries of the elongated resulting in the nucleation of lenticular carbides rather than carbon migration across the whole equiaxed ferrite band. In HAB, adjacent lenticular carbides act as carbon sinks driving carbon migration from the equiaxed grains to the carbides. This depletes the equiaxed band prior to the formation of elongated grains, hence no new lenticular carbides are formed in HAB unlike LAB.

This study has successfully recorded the gradual RCF-induced transformation of LAB and HAB in the subsurface microstructure of ACBBs. It is concluded that the formation of both LAB and HAB is influenced by energy build up and release in the steel microstructure driven by recurring recrystallization and recovery mechanisms that occurs during bearing operation. However, the stress components responsible for such an energy build-up and the orientation of such components remain unclear. Modelling of the initial local microstructure (parent microstructure and DER) prior to LAB formation and the initial local microstructure prior to HAB formation (closely-packed LAB consisting of ferrite bands and lenticular carbides) may assist in resolving the stress/strain components responsible for these transformations and their orientations.

Declaration of Competing Interest

None.

Acknowledgement

This research has been co-funded by ESPRC (EP/N509747/1) and Schaeffler Technologies AG & Co. KG, Schweinfurt, Germany.

References

[1] H. Fu, W. Song, E.I. Galindo-Nava, P.E.J. Rivera-Dıáz-del-Castillo, Strain-induced martensite decay in bearing steels under rolling contact fatigue: modelling and atomic-scale characterisation, Acta Mater. 139 (2017) 163–173.
[2] M. El Laithy, L. Wang, T.J. Harvey, B. Vierneusel, M. Correns, T. Blass, Further understanding of rolling contact fatigue in rolling element bearings-a review, Tribol. Int. (2019) 105849.
[3] M. El Laithy, L. Wang, T. Harvey, B. Vierneusel, Re-investigation of dark etching regions and white etching bands in SAE5 2100 bearing steel due to rolling contact fatigue, Int. J. Fatigue 136 (2020) 105591.
[4] A. Voskamp, Material Response to rolling contact loading, J. Tribol. 107 (1985) 359–364.
[5] H.P.C.O. Swahn, P.C. Becker, O. Vingsbo, Martensite decay during rolling contact fatigue in ball bearings, Metall. Trans. A 7 (1976) 1099–1110.
[6] A. Warhadpande, F. Sadeghi, R.D. Evans, Microstructural alterations in bearing steels under rolling contact fatigue Part 1—Historical overview, Tribol. Trans. 56 (2013) 349–358.
[7] N.H. Forster, L. Rosado, W.P. Ogden, H.K. Trivedi, Rolling contact fatigue life and spall propagation characteristics of AISI M50, M50 NiL, and AISI 52100, Part III: metallurgical examination, Tribol. Trans. 53 (2009) 52–59.
[8] A.P. Voskamp, Microstructural stability and bearing performance, Bearing Steel Technology, ASTM International, 2002.
[9] H. Fu, P.E.J. Rivera-Dıáz-del-Castillo, A unified theory for microstructural alterations in bearing steels under rolling contact fatigue, Acta Mater. 155 (2018) 43–55.
[10] V. Šmeļova, A. Schwedt, L. Wang, W. Holweger, J. Mayer, Electron microscopy investigations of microstructural alterations due to classical Rolling Contact Fatigue (RCF) in martensitic AISI 52100 bearing steel, Int. J. Fatigue 98 (2017) 142–154.
[11] H. Fu, P.E.J. Rivera-Dıáz-del-Castillo, Evolution of white etching bands in 100Cr6 bearing steel under rolling contact-fatigue, Metals 9 (2019) 491.
[12] N. Maharjan, W. Zhou, Y. Zhou, Micro-structural study of bearing material failure due to rolling contact fatigue in wind turbine gearbox, in: Proceedings of the International Symposium on Current Research in Hydraulic Turbines, Dhulikhel, Nepal, Kathmandu University, 2016.
[13] M. El Laithy, L. Wang, T. Harvey, B. Vierneusel, Semi-empirical model for predicting LAB and HAB formation in Bearing Steels, Int. J. Fatigue (2021) 106230.
[14] J. Buchwald, R.W. Heckel, An analysis of microstructural changes in 52100 steel bearings during cyclic stressing(Microstructural changes in 52100 steel bearing inner rings during cyclic stressing, obtaining thickening rate data on white-etching regions and lenticular carbides), ASM Trans. Q. 61 (1968) 750–756.
[15] I.A. Polonsky, L.M. Keer, On white etching band formation in rolling bearings, J. Mech. Phys. Solids 43 (1995) 637–669.
[16] D. Markus, T. Werner, Influence of sulfur inclusion content on rolling contact fatigue life, Bearing Steel Technol. 10 (2014) 83–99.
[17] D. Markus, T. Werner, Influence of sulfur inclusion content on rolling contact fatigue life, Bearing Steel Technol. 10 (2014) 83–99.
[18] Kenneth Kanayo Alaneme, Eloho Anita Okotete, Recrystallization mechanisms and microstructure development in emerging metallic materials: a review, J. Sci. 4 (2019) 19–33.
[19] L. Ryde, Application of EBSD to analysis of microstructures in commercial steels, Mater. Sci. Technol. 22 (11) (2006) 1297–1306.
[20] J. Kang, P. Rivera-Díaz-del-Castillo, Carbide dissolution in bearing steels, Comput. Mater. Sci. 67 (2013) 364–372.
[21] V. Gavriljuk, Decomposition of cementite in pearlitic steel due to plastic deformation, Mater. Sci. Eng. 345 (2013) 81–89.
[22] J. Languillaume, G. Kapelski, B. Baudelet, Cementite dissolution in heavily cold drawn pearlitic steel wires, Acta Mater. 45 (3) (1997) 1201–1212.
[23] X. Sauvage, J. Copreaux, F. Danoix, D. Blavette, Atomic-scale observation and modelling of cementite dissolution in heavily deformed pearlitic steels, Philos. Mag. A 80 (4) (2000) 781–796.
[24] F. Humphreys, M. Hatherly, Recovery after deformation, Recrystall. Related Annealing Phenomena (2004) 199–244.
[25] B. Chen, L. Zhu, Y. Xin, J. Lei, Grain rotation in plastic deformation, Quantem Beam Sci. 17 (3) (2019).
[26] I.A. Ovid'ko, Plastic deformation mechanisms in nanocrystalline metallic materials, J. Mech. Behav. Mater. 22 (2012).
[27] S.V. Bobylev, I.A. Ovid'ko, Stress-driven rotations of high-angle grain boundaries in nanocrystalline materials, Rev. Adv. Mater. Sci. 35 (2013) 25–38.
[28] D. Moldovan, D. Wolf, S. Phillpot, A. Haslam, Grain rotation as a mechanism of grain growth in nanocrystalline materials, Trends Nanoscale Mech. (2003) 35–59.
[29] H. Fu, "Microstructural alterations in bearing steels under rolling contact fatigue," 2017.
[30] O. Zwirlein, H. Schlicht, Rolling contact fatigue mechanisms—accelerated testing versus field performance, Rolling Contact Fatigue Testing of Bearing Steels, ASTM International, 1982.
[31] F. Sadeghi, B. Jalalahmadi, T.S. Slack, N. Raje, N.K. Arakere, A review of rolling contact fatigue, J. Tribol. 131 (2009) 041403.
[32] J.J. Bush, W.L. Grube, G.H. Robinson, Microstructural and residual stress changes in hardened steel due to rolling contact, Trans. ASM 54 (1961) 390–412.
[33] S. Borgese, A study of the growth mechanism of lenticular carbides in cyclically stressed 52100 steel, J. Lubr. Technol. 92 (1970) 54–58.
[34] R. Österlund, O. Vingsbo, Phase changes in fatigued ball bearings, Metall. Trans. A 11 (1980) 701–707.
[35] Y. Liab, M. Herbig, S. Gotoa, D. Raabea, Atomic scale characterization of white etching area and its adjacent matrix in a martensitic 100Cr6 bearing steel, Mater. Charact. 123 (2017) 349–353.
[36] H. Danielsen, F. Gutiérrez, K. Guzmán, Y. Li, J. Wu, G. Jacobs, G. Burghardt, S. Fæster, H. Alimadadi, S. Goto, D. Raabe, R. Petrov, Multiscale characterization of White Etching Cracks (WEC) in a 100Cr6 bearing from a thrust bearing test rig, Wear 370-371 (2017) 73–82.
[37] A. Warhadpande, F. Sadeghi, R.D. Evans, Microstructural alterations in bearing steels under rolling contact fatigue: part 2—diffusion-based modeling approach, Tribol. Trans. 57 (2013) 66–76.
[38] J.M. Beswick, Measurement of C levels in structurally transformed SAE 52100 ball-bearing steel by microprobe analysis, Prakt. Metallogr. 12 (1975) 200–206.
[39] P. Chen, S.C. Mao, Y. Liu, F. Wang, Y.F. Zhang, Z. Zhang, X.D. Han, In-situ EBSD study of the active slip systems and lattice rotation behavior of surface grains in aluminum alloy during tensile deformation, Mater. Sci. Eng. 580 (2013) 114–124.